Relativistic multireference many-body perturbation-theory calculations on the multiple openshell states in siliconlike Ar and aluminumlike Fe ions

Marius J. Vilkas and Yasuyuki Ishikawa*
Department of Chemistry, University of Puerto Rico, P.O. Box 23346 San Juan, Puerto Rico 00931-3346, USA
(Received 20 March 2003; published 9 July 2003)

Energies of the ground and a number of even- and odd-parity excited states of multi-valence-electron ions have been computed by a computational method in the framework of relativistic multireference many-body perturbation theory. Relativistic multireference perturbation calculations are reported for the ground and over 80 low-lying odd- and even-parity excited states of siliconlike argon (Ar^{4+}) and aluminumlike iron (Fe^{13+}) to demonstrate the unprecedented accuracy of the method. The theory deviates from experiment by less than 0.2% for all but a few excited levels in siliconlike argon. For the more highly ionized aluminumlike iron, the deviations are reduced to within 0.06%. Theoretical magnetic dipole and electric quadrupole transition rates of the lowest-lying $^2P^o_{3/2}$ state of aluminumlike Fe and Mn are evaluated, and lifetimes are compared with a recent ion trap experiment.

DOI: 10.1103/PhysRevA.68.012503 PACS number(s): 31.15.Ar, 31.15.Md, 31.15.Ne, 31.25.Jf

I. INTRODUCTION

Precision wavelength measurements on multiple openshell ions using electron-beam ion traps (EBITs) as spectroscopic sources of ions [1] provide a sensitive means of testing atomic many-body theory calculations including relativistic, electron correlation, and quantum electrodynamic (QED) effects. The recent development of experimental techniques for optical observation at a heavy-ion storage ring [2] has provided lifetime measurements of forbidden transitions in high precision, at the 1% uncertainty level. Precisely measured $M1$ transition energies and lifetimes, provide experimental tests of theoretical predictions of $M1$ transitions. Only a small number of *ab initio* theoretical studies of $M1$ and $E2$ transitions have been reported in the past three decades [3–9]. $M1$ and $E2$ transition probabilities involve, respectively, the third- and the fifth-power dependence on transition energy, mandating high accuracy calculations of term energy separations. Thus, an accurate relativistic many-body algorithm must be brought to bear on the prediction of the transition energies and transition rates.

Relativistic multiconfiguration Dirac-Fock (MCDF) self-consistent field (SCF) calculations have been widely employed to calculate transition energies and transition rates. Relativistic MCDF SCF and configuration interaction (CI) methods are most effective in treating nondynamic correlation, a near degeneracy effect in the valence shells. They often fail, however, to accurately account for the bulk of dynamic correlation, a short-range effect that arises from electron-electron interaction, as the methods are inherently limited by the number of configurations that can be included. Thus these methods often fail to provide accurate transition energies, and a semiempirical adjustment of the computed transition rates is required to obtain agreement with experiment. Recently, a precise and efficient relativistic CI + many-body perturbation theory (MBPT) method for systems with two valence-shell electrons has been implemented and applied to Be, Mg, Ca, and Sr to account for nondynamic correlation in the valence-shell electrons by CI, and dynamic correlation between the valence and core electrons by MBPT [10,11]. With proper account taken of nondynamic correlation in the two-electron valence shell, the combined CI+MBPT method is capable of predicting term energy separations typically within a 1% deviation from the experiment [11].

Multiple openshell systems with more than two valence electrons give rise to complex spectra because of the large number of nearly degenerate multiplet states that arise from the multiple openshells. In an earlier study, a relativistic multireference Møller-Plesset (MR-MP) perturbation theory based on the $\mathcal{J}$-averaged MCDF SCF was implemented and successfully applied to ions of silicon isoelectronic sequences [12]. In that study, the $\mathcal{J}$-averaged energy over the $^3P_{\mathcal{J}}$ ($\mathcal{J}=0,1,2$) fine-structure terms was optimized by MCDF SCF followed by state-specific second-order MR-MP to obtain highly accurate fine-structure separations and lifetimes. In the present study, we generalize the previous study and develop an efficient, state-averaged MCDF SCF+state-specific MR-MP procedure to obtain accurate term energy separations for openshell systems with multiple valence-shell electrons. Relativistic multireference perturbation calculations are reported for the ground and over 80 low-lying odd- and even-parity excited states of siliconlike argon and aluminumlike iron to demonstrate the high accuracy attainable for systems with multiple valence electrons. Theoretical $M1$ transition rates of the lowest-lying $^2P^o_{3/2}$ state of alminumlike iron (Fe^{13+}) and manganese (Mn^{12+}) ions are evaluated and compared with recent ion trap experiments [13–15]. The relativistic MR-MP perturbation theory accounts for relativistic, nondynamic, and dynamic Dirac-Coulomb and Breit correlation energies and Lamb shift corrections. It can provide accurate transition energies and transition rates among multiplet states of atoms for a broad range of ionizations.

In the following section, the method of state-averaged

*Electronic address: ishikawa@rrpac.upr.clu.edu

 ©2003 The American Physical Society

MCDF SCF+state-specific MR-MP and theoretical transition probabilities are briefly outlined to contrast the difference between the present and earlier approaches. In Sec. III, the results of the MR-MP calculations on siliconlike argon and aluminumlike iron are compared with the experiment.

II. METHODS

A. Relativistic multireference many-body perturbation theory

The effective N-electron Hamiltonian (in atomic units) for the development of our relativistic MR-MP algorithm is taken to be the relativistic "no-pair" Dirac-Coulomb-Breit (DCB) Hamiltonian [16,17],

$$H^{+}_{DCB}=\sum_i h_D(i)+\mathcal{L}_+\left(\sum_{i>j}\frac{1}{r_{ij}}+B_{ij}\right)\mathcal{L}_+$$

with

$$B_{ij}=-\tfrac{1}{2}[\boldsymbol{\alpha}_i\cdot\boldsymbol{\alpha}_j+(\boldsymbol{\alpha}_i\cdot\mathbf{r}_{ij})(\boldsymbol{\alpha}_j\cdot\mathbf{r}_{ij})/r_{ij}^2]/r_{ij}.$$

Here $h_D(i)$ is the Dirac one-electron Hamiltonian. The DCB Hamiltonian is covariant to first order and increases the accuracy of calculated fine-structure splittings and inner-shell binding energies. Higher-order QED effects appear first in order α^3. The nucleus is modeled as a sphere of uniform proton charge distribution. $\mathcal{L}_+=L_+(1)L_+(1)\cdots L_+(1)$, where $L_+(1)$ is the projection operator onto the space $D^{(+)}$ spanned by the positive-energy eigenfunctions of the matrix Dirac-Fock-Breit (DFB) SCF equation [17]. $\mathcal{L}_+$ is the projection operator onto the positive-energy space $\mathfrak{D}^{(+)}$ spanned by the N-electron configuration-state functions (CSFs) constructed from the positive-energy eigenfunctions of the matrix DFB SCF. It takes into account the field-theoretic condition that the negative-energy states are filled. The eigenfunctions of the matrix DFB SCF equation clearly separate into two discrete manifolds $D^{(+)}$ and $D^{(-)}$, respectively, of positive- and negative-energy states. As a result, the positive-energy projection operators can be accommodated easily in many-body calculations. The formal conditions on the projection are automatically satisfied when only the positive-energy spinors are employed. The N-electron eigenfunctions of the no-pair DCB Hamiltonian are approximated by a linear combination of M configuration-state functions, $\{\Phi_I^{(+)}(\gamma_I\mathcal{J}\pi);I=1,2,\ldots,M\}$ in $\mathfrak{P}^{(+)}$, constructed from positive-energy eigenfunctions of the matrix multiconfiguration Dirac-Fock-Breit (MCDFB) SCF equation [17],

$$\psi_K(\gamma_K\mathcal{J}\pi)=\sum_I^M C_{IK}\Phi_I^{(+)}(\gamma_I\mathcal{J}\pi). \tag{1}$$

The MCDFB SCF wave function $\psi_K(\gamma_K\mathcal{J}\pi)$ is an eigenfunction of the angular momentum and parity operators with total angular momentum $\mathcal{J}$ and parity π. γ denotes a set of quantum numbers other than $\mathcal{J}$ and π necessary to specify the state uniquely. The total DCB energy of the general state represented by the MC wave function $\psi_K(\gamma_K\mathcal{J}\pi)$ can be expressed as

$$E^{MC}(\gamma_K\mathcal{J}\pi)=\sum_{IJ}^{\mathfrak{P}(+)} C_{IK}C_{JK}\langle\Phi_I^{(+)}(\gamma_I\mathcal{J}\pi)|H^{+}_{DCB}|\Phi_J^{(+)}(\gamma_J\mathcal{J}\pi)\rangle. \tag{2}$$

Here, it is assumed that $\psi_K(\gamma_K\mathcal{J}\pi)$ and $\Phi_J^{(+)}(\gamma_J\mathcal{J}\pi)$ are normalized.

Given a trial orthonormal set of one-particle radial spinors $\{\phi^{(0)}_{n_q\kappa_q}(r)\}(\in D^{(+)}\cup D^{(-)})$, the optimum occupied electronic radial spinors $\{\phi^{(+)}_{n_p\kappa_p}(r)\}(\in D^{(+)})$ can be found by a unitary transformation $\mathbf{U}=1+\mathbf{T}$ via

$$\begin{aligned}\phi^{(+)}_{n_p\kappa_p}(r)&=\frac{1}{r}\begin{pmatrix}P_{n_p\kappa_p}(r)\\ Q_{n_p\kappa_p}(r)\end{pmatrix}\\&=\sum_{q\in D^{(+)}\cup D^{(-)}}^{2N_\kappa}\phi^{(0)}_{n_q\kappa_q}(r)U_{qp}\\&=\sum_q^{2N_\kappa}\phi^{(0)}_{n_q\kappa_q}(r)(T_{qp}+\delta_{qp}).\end{aligned}$$

Here, the summation extends over both N_κ negative energy and N_κ positive energy spinors. $P_{n_p\kappa_p}(r)$ and $Q_{n_p\kappa_p}(r)$ are the large and small radial components and are expanded in N_κ G spinors, $\{\chi^L_{\kappa i}\}$ and $\{\chi^L_{\kappa i}\}$, that satisfy the boundary conditions associated with the finite nucleus [18],

$$P_{n\kappa}(r)=\sum_i^{N_\kappa}\chi^L_{\kappa i}\xi^L_{ki}\quad\text{and}\quad Q_{n\kappa}(r)=\sum_i^{N_\kappa}\chi^S_{\kappa i}\xi^S_{ki}.$$

Here $\{\xi^L_{ki}\}$ and $\{\xi^S_{ki}\}$ are linear variation coefficients. Second-order variation of the MCDF energy [Eq. (2)] with respect to the parameters $\{T_{qp}\}$ and configuration mixing coefficients $\{C_{IK}\}$ leads to the Newton-Raphson (NR) equations for the state-specific second-order MCDF SCF,

$$\begin{pmatrix}g^o_{pe}\\ g^c_\gamma\end{pmatrix}+\sum_{qf\gamma''}\begin{pmatrix}h^{oo}_{pe,gf} & h^{oc}_{pe,\gamma''}\\ h^{co}_{\gamma',gf} & h^{cc}_{\gamma',\gamma''}\end{pmatrix}\begin{pmatrix}T_{qf}\\ B_{\gamma''}\end{pmatrix}=\begin{pmatrix}0\\0\end{pmatrix}.$$

Here g^o_{pe}, g^c_γ, $h^{oo}_{pe,gf}$, etc., are as defined in previous work [19]. Intermediate coupling is built in through the MC DFB SCF process. The quadratically convergent NR algorithm for relativistic MCDFB SCF calculations has been discussed in detail [19].

In an earlier study [20], state-specific MCDFB SCF calculations were performed, followed by state-specific MR-MP calculations. In the present study, second-order variation of the state-averaged energy $\Omega_{state\text{-}ave}$ given below [Eq. (3)] is taken with respect to the parameters $\{T_{qp}\}$ and configuration mixing coefficients $\{C_{IK}\}$, leading to the Newton-Raphson equations for the state-averaged second-order MCDFB SCF. These state-averaged second-order MCDFB equations yield a single set of spinors for the ground and all low-lying even- and odd-parity excited (γ, $\mathcal{J}$, π) levels, including $^{2S+1}L_{\mathcal{J}}$

fine-structure states, for which subsequent state-specific MR-MP perturbation calculations are to be performed:

$$\Omega_{state\text{-}ave} = \sum_{\gamma_K \mathcal{J}\pi} E^{MC}(\gamma_K \mathcal{J}\pi) = \sum_{\gamma_K \mathcal{J}\pi} \sum_{IJ}^{\mathfrak{P}(+)} C_{IK} C_{JK} \langle \Phi_I^{(+)} \times (\gamma_I \mathcal{J}\pi) | H_{DCB}^{+} | \Phi_J^{(+)}(\gamma_J \mathcal{J}\pi) \rangle, \quad (3)$$

where summation indices, γ, $\mathcal{J}$, and π, run over the ground and excited states including a set of $^{2S+1}L_{\mathcal{J}}$ ($\mathcal{J}=|L-S|, \ldots, |L+S|$) fine-structure states. S and L are the spin and orbital angular-momentum quantum numbers. To remove the arbitrariness of the matrix MCDFB SCF spinors and density weighting [21,22], the canonical SCF spinors are transformed into natural spinors $\{\omega_{n_p\kappa_p}^{(+)}\}$ for subsequent perturbation calculations.

Conventional state-specific MCDFB SCF has the disadvantage that each state has its own set of core and valence spinors, which leads to a slightly unbalanced representation of dynamic correlation corrections to term energy separations in subsequent state-specific second-order perturbation calculations. This small imbalance in representing dynamic correlation among states in finite-order perturbation theory restricts the accuracy of calculated term energy separations. Note that in all-order perturbation theory, this imbalance would vanish. In contrast, state-averaged MCDFB SCF followed by state-specific second-order MR-MP perturbation theory has the advantage that the state-averaged MCDFB defines a single set of spinors for all states included. The single set of spinors provides, in finite-order perturbation theory, a well-balanced representation of dynamic correlation energy corrections on term energy separations. In recent CI + second-order MBPT calculations on two-valence-electron systems [10,11], a single set of spinors generated by a V^{N-2} potential was employed to accurately account for nondynamic correlation by valence-shell CI, and remaining dynamic correlation by second-order MBPT. Fock-space relativistic coupled cluster theory [23] also employs a single set of spinors generated from a V^{N-2} potential in closedshell Dirac-Fock calculations.

The no-pair DCB Hamiltonian H_{DCB}^{+} is decomposed into two parts, the unperturbed Hamiltonian H_0 and perturbation V, following Møller and Plesset [21,22,24],

$$H_{DCB}^{+} = H_0 + V = \sum_i^N F(i) + V,$$

where the unperturbed model Hamiltonian H_0 is a sum of one-body operators, $F = \Sigma_{p \in D(+)} |\omega_{n_p\kappa_p}^{(+)}\rangle \varepsilon_p \langle \omega_{n_p\kappa_p}^{(+)}|$; ε_p is the Lagrange multiplier, or orbital energy, for occupied spinor $\omega_{n_p\kappa_p}^{(+)}$. The one-body operator in the positive-energy virtual space $V(+)$ is defined by

$$F = \sum_{p \in V(+)} |\omega_{n_p\kappa_p}^{(+)}\rangle \langle \omega_{n_p\kappa_p}^{(+)}| f_{av} |\omega_{n_p\kappa_p}^{(+)}\rangle \langle \omega_{n_p\kappa_p}^{(+)}|,$$

where

$$f_{av} = h_D + \sum_p^{occ} \tilde{n}_p (J_p - K_p).$$

The generalized fractional occupation $\tilde{n}_p$ is related to diagonal matrix elements of the first-order reduced density matrix constructed in natural spinors by

$$\tilde{n}_p = D_{pp} = \sum_{\gamma_K \mathcal{J}\pi} \sum_I^{\mathfrak{P}(+)} C_{IK} C_{IK} n_{n_p\kappa_p}[I],$$

and E_I^{CSF} is a sum of the products of one-electron energies defined by ε_q and an occupation number $n_{n_q\kappa_q[I]}$,

$$E_I^{CSF} = \sum_q^{D(+)} \varepsilon_q^{+} n_{n_q\kappa_q[I]},$$

where $n_{n_p\kappa_p}[I]$ is the occupation number of the κ-symmetry shell in the CSF $\Phi_I(\gamma_I \mathcal{J}\pi)$. J_p and K_p are the usual Coulomb and exchange operators constructed in natural spinors.

The application of the Rayleigh-Schrödinger perturbation theory provides order-by-order expressions of the perturbation series for the zero-order state approximated by $|\psi_K(\gamma_K \mathcal{J}\pi)\rangle$. The second-order energy is given by

$$E_K^{(2)} = \langle \psi_K(\gamma_K \mathcal{J}\pi) | V \mathcal{R} V | \psi_K(\gamma_K \mathcal{J}\pi) \rangle. \quad (4)$$

Here $\mathcal{R}$ is the resolvent operator,

$$\mathcal{R} = \mathcal{Q}^{(+)}/(E^{CSF} - H_0), \quad (5)$$

$$\mathcal{Q}^{(+)} = \sum_I^{\mathfrak{Q}(+)} |\Phi_I^{(+)}(\gamma_I \mathcal{J}\pi)\rangle \langle \Phi_I^{(+)}(\gamma_I \mathcal{J}\pi)|. \quad (6)$$

The projection operator $\mathcal{Q}^{(+)}$ projects onto the subspace spanned by a residual space $\mathfrak{Q}^{(+)} = \mathfrak{D}^{(+)} - \mathfrak{P}^{(+)}$. All the perturbation corrections beyond first order describe relativistic electron correlation [25] including cross relativistic-correlation effects, the relativistic many-body shift. When the effective electron-electron interaction is approximated by the instantaneous Coulomb interaction $1/r_{12}$, relativistic electron correlation is termed DC correlation [26]. Inclusion of the frequency-independent Breit interaction in the effective electron-electron interaction yields the no-pair DCB Hamiltonian, and the relativistic electron correlation arising from the DCB Hamiltonian is the DCB correlation [26]. The essential features of the theory are its treatment of the nondynamical correlation in zero order through state-averaged MCDFB SCF, and recovery of the remaining correlation, which is predominantly dynamic pair correlation, by second-order perturbation theory.

Radiative corrections, Lamb shifts, were estimated for each state by evaluating the electron self-energy and vacuum polarization following an approximation scheme discussed by Indelicato, Gorceix, and Desclaux [27]. The code described in Refs. [27,28] was adapted to our basis set expansion calculations for this purpose. All necessary radial inte-

grals were evaluated analytically. In this scheme [28], the screening of the self-energy is estimated by integrating the charge density of a spinor to within a short distance of the origin, typically 0.3 Compton wavelength. The ratio of the integral computed with a MCDFB SCF spinor and that obtained from the corresponding hydrogenic spinor is used to scale the self-energy correction for a bare nuclear charge, which has been computed by Mohr [29].

B. Transition probabilities

Many-electron multipole transition operators T^{ϑ}_{JM} for the magnetic ($\vartheta=E$) and electric ($\vartheta=M$) multipoles may be given in second-quantized form [30,12],

$$T^{\vartheta}_{JM}=\sum_{ij}\ \langle t^{\vartheta}_{JM}\rangle_{ij}a^{+}_{i}a_{j}\,.$$

Here $t^{\vartheta}_{JM}(\mathbf{r},w)$ are one-particle multipole transition operators [12]. The absorption probability $\langle B\rangle_{K\rightarrow K'}$ per unit time of transition between states $|\psi_K(\gamma_K\mathcal{J}\pi)\rangle$ and $|\psi_{K'}(\gamma_{K'}\mathcal{J}'\pi')\rangle$ with transition energy $\Delta E=hw=E_{K'}-E_K$ is equal to the spontaneous emission probability $\langle A\rangle_{K'\rightarrow K}$ and is expressed as

$$\langle B^{\vartheta J}\rangle_{K\rightarrow K'}=2\alpha w\frac{(2J+1)(J+1)}{(2\mathcal{J}+1)J}[\langle T^{\vartheta}_{J}\rangle_{K'K}]^2$$
$$=\langle A^{\vartheta J}\rangle_{K'\rightarrow K}\,.$$

In the lowest order of the Rayleigh-Schrödinger perturbation theory, the multipole transition amplitude between states K and K' is

$$\langle T^{\vartheta}_{J}\rangle^{(0)}_{KK'}=\langle\psi_K(\gamma_K\mathcal{J}\pi)|T^{\vartheta}_{JM}|\psi_{K'}(\gamma_{K'}\mathcal{J}'\pi')\rangle$$
$$=\sum_{IL}\ C_{IK}C'_{IK'}\langle|\Phi^{(+)}_{I}(\gamma_I\mathcal{J}\pi)|T^{\vartheta}_{JM}|\Phi'^{(+)}_{L}(\gamma_L\mathcal{J}'\pi')\rangle,$$

and using the order-by-order expressions of the perturbation series for the state approximated by MCDF SCF wave function $\psi_K(\gamma_K\mathcal{J}\pi)$ of Eq. (1), the next-order transition amplitude is

$$\langle T^{\vartheta}_{J}\rangle^{(1)}_{KK'}=\langle\psi^{(1)}_{K}(\gamma_K\mathcal{J}\pi)|T^{\vartheta}_{JM}|\psi_{K'}(\gamma_{K'}\mathcal{J}'\pi')\rangle$$
$$+\langle\psi_K(\gamma_K\mathcal{J}\pi)|T^{\vartheta}_{JM}|\psi^{(1)}_{K'}(\gamma_{K'}\mathcal{J}'\pi')\rangle,$$

where the first-order wave function is defined as

$$|\psi^{(1)}_{K}(\gamma_K\mathcal{J}\pi)\rangle=\mathcal{R}V|\psi_K(\gamma_K\mathcal{J}\pi)\rangle.$$

The first-order transition amplitude can be expressed in terms of CSFs in the following way:

$$\langle T^{\vartheta}_{J}\rangle^{(1)}_{KK'}=\sum_{L=M+1}^{\mathfrak{Q}(\pm)}\sum_{I,I'=1}^{\mathfrak{P}(+)}C_{IK}C'_{I'K'}\left[\frac{\langle\Phi^{(+)}_{I}|V|\Phi^{(\pm)}_{L}\rangle\langle\Phi^{(\pm)}_{L}|T^{\vartheta}_{JM}|\Phi'^{(+)}_{I'}\rangle}{E^{CSF}_{I}-E^{CSF}_{L}}+\frac{\langle\Phi^{(+)}_{I}|T^{\vartheta}_{JM}|\Phi'^{(\pm)}_{L}\rangle\langle\Phi'^{(\pm)}_{L}|V|\Phi'^{(+)}_{I'}\rangle}{E^{CSF}_{I'}-E^{CSF}_{L}}\right].$$

Summation L over intermediate states $\Phi^{(\pm)}_{L}$ includes both the positive- $[\mathfrak{Q}(+)]$ and negative- $[\mathfrak{Q}(-)]$ energy subspaces [4]. With the summation extended to negative-energy subspace, $E1$ and $E2$ transition probabilities computed in the velocity gauge approach the values computed in the length gauge. One-electron reduced matrix elements are frequency dependent through the spherical Bessel functions $j_J(kr)$. The corrections arising from approximate photon frequency may be eliminated semiempirically using experimental transition energies. In the present study, transition energies (and photon frequencies $\omega^{(0+1+2)}$) calculated by the MR-MP second-order perturbation theory are close to the experimental values, and terms arising from corrections to the photon frequency $\delta\omega=\omega^{expt}-\omega^{(0+1+2)}$ in both zero- and first-order transition amplitudes are significantly smaller and may be neglected. When the first-order corrections to transition probabilities are calculated using the second-order MR-MP transition energies, however, the zero-order transition amplitude must also be recalculated using the frequency $\omega^{(0+1+2)}$.

The large and small radial components of the Dirac spinors of symmetry κ are expanded in sets of even-tempered Gaussian-type functions (GTFs) that satisfy the boundary conditions associated with the finite nucleus [18]. The speed of light is taken to be 137.035 989 5 a.u. throughout this study. The GTFs that satisfy the boundary conditions associated with the finite nucleus are automatically kinetically balanced. For all the systems studied, even-tempered basis sets of $26s24p20d18f15g15h15i15j$ G spinors were employed. The order of the partial-wave expansion ($L_{\max}$), the highest angular momentum of the spinors included in the virtual space, is $L_{\max}=7$ throughout this study. The nuclei were modeled as spheres of uniform proton charge in all calculations. Atomic masses for the Ar^{4+} ($Z=18$) and Fe^{13+} ($Z=26$) ions are, respectively, 39.948 and 55.847. All electrons have been included in the MR-MP perturbation-theory calculations to calculate accurately the effects of relativity on electron correlation.

III. RESULTS AND DISCUSSION

A. Term energy and fine-structure separations in siliconlike argon

Astrophysical interest in intercombination and forbidden transitions in low charge state ions, such as Ar^{4+}, has in-

TABLE I. Contributions to the energies (atomic units) of states of siliconlike Ar^{4+}. These include MCDFB, second-order Dirac-Coulomb-Breit correction $E^{(2)}_{DCB}$, and Lamb shift correction.

State	E_{MCDFB}	$E^{(2)}_{DCB}$	Lamb shift
$3s^2 3p^2\ ^3P_0$	−523.537737	−0.478410	0.008695
$3s3p^3\ ^5S^o_2$	−523.165973	−0.461717	0.008655
$3s^2 3p3d\ ^3F^o_2$	−522.669254	−0.495622	0.009056
$3p^4\ ^3P_2$	−522.331204	−0.480197	0.008075
$3s3p^2 3d\ ^5F_1$	−522.289738	−0.474874	0.008280
$3s^2 3d^2\ ^3F_4$	−521.526548	−0.562307	0.008572

creased in recent years as earth-orbiting instrumentation has expanded the range of detectable radiation into the x-ray region [31]. We have calculated the energies of the ground and a number of even- and odd-parity excited states of siliconlike argon by state-averaged MCDFB SCF followed by relativistic multireference many-body perturbation theory. MCDFB SCF employs a restricted active space within the $n=3$ ($3s_{1/2}$, $3p_{1/2}$, $3p_{3/2}$, $3d_{3/2}$, $3d_{5/2}$) spinor subspace. In the MCDFB SCF calculations, the $1s_{1/2}$, $2s_{1/2}$, and $2p_{1/2,3/2}$ spinors were kept fully occupied, and the remaining four electrons were treated as active electrons for generating the restricted active space CSFs by single and double excitation from the ground $3s^2_{1/2}3p^2_{1/2}$ CSF. The numbers of CSFs generated were, respectively, 22, 34, 52, 36, 28, and 10 for the $\mathcal{J}=0$, 1, 2, 3, 4, and 5 even-parity states, while for the odd-parity $\mathcal{J}=0$, 1, 2, 3, 4 states they were, respectively, 13, 34, 40, 33, and 20. All these states were included in the state-averaged energy [Eq. (3)]. Following the state-averaged MCDFB SCF calculations, state-specific MR-MP calculations were carried out on each of the states, employing a single, orthonormal set of spinors. Table I displays the computed MCDFB SCF energies, E_{MCDFB}, Lamb shifts, and second-order DCB correlation corrections, $E^{(2)}_{DCB}$, of representative even- and odd-parity states of Ar^{4+}.

In Table II, a detailed comparison of the theoretical and experimental data is made for the term energy separations (ΔE) of the lowest 31 excited states relative to the ground $\mathcal{J}=0$ ($3s^2 3p^2\ ^3P_0$) state. In the first column of the Table, 32 states, including the ground state, are numbered in order of increasing energy. Spectroscopic term symbols are given in the second column. Theoretical MCDFB term energy separations and fine-structure (FS) intervals computed in the present study, by Huang [7], and by Kohstall *et al.* [33] are displayed in the third through eighth columns, respectively, of the table. The ninth and tenth columns contain the term energy separations and fine-structure intervals computed in the MR-MP calculations. The term energy separations were computed by subtracting the total energy of the ground $\mathcal{J}=0$ ($3s^2 3p^2\ ^3P_0$) state from those of the excited levels. Values in parentheses adjacent to the term energy separations are the percentage deviations between the experiment and MR-MP theory. Experimental term energy separations and fine-structure intervals compiled in the National Institute of Standards and Technology (NIST) Atomic Spectra Database [34] are reproduced in the last column for comparison. Theoretical MCDFB and MR-MP fine-structure intervals of the lowest $^3P_1$ ($\mathcal{J}=1$) and $^3P_2$ ($\mathcal{J}=2$) were computed by subtracting the total MCDFB and MR-MP energies of the ground $\mathcal{J}=0$ ($3s^2 3p^2\ ^3P_0$) state from those of the $\mathcal{J}=1$ and 2 levels.

The MR-MP term energy separations shown in Table II demonstrate that the theory deviates from the experiment by less than 0.2% for all but a few excited levels. The theoretical term energy separations are indeed accurate enough so that the scrutiny of experimental results is warranted when deviations are 1% or larger. Deviations (in cm^{-1}) between theory and experiment for the lowest 31 excited levels are plotted against the state number in Fig. 1 to exemplify the accuracy of the MR-MP theory, and a few notable discrepancies are revealed. Among the excited levels that exhibit significant deviation is the $3s3p^3\ ^5S^o_2$ state (state number 6 in Table II) where the theory deviates from the experiment by as much as 2%. Here the experimental excitation energy adopted in the NIST Atomic Spectra Database is suspect. A beam-foil spectroscopy experiment [35], however, measured this excitation energy to be $85\,900\pm80$ cm^{-1}, and isoelectronic fit with low-order polynomial gave 85 823 cm^{-1} [36] in excellent agreement with our theoretical estimate, 85819 cm^{-1}. Figure 1 also reveals large deviations for the $3p^4\ ^1D_2$ and $3p^4\ ^1S_0$ terms. The experiment assigns the level 228519 cm^{-1} above the ground level as the even parity $^1D_2$. This term appears in the midst of a manifold of low-lying $3s^2 3p3d$ odd-parity states, while the theory estimates it to appear 271 405 cm^{-1} above the ground level, well within the manifold of $3p^4$ even-parity states. The level that appears at 324 864 cm^{-1} above ground has been assigned as the even parity $^1S_0$, the while theory estimates this state to appear well below at 311 996 cm^{-1}. Because of their unusually large deviations, we would argue that the experimental assignments of the $3p^4\ ^1S_0$ and $^1D_2$ terms are suspect.

Another significant discrepancy lies in the $3s3p^3\ ^3P^o_{\mathcal{J}=0,1,2}$ fine-structure levels. According to data in the NIST compilation, the $3s3p^3\ ^3P^o_0$ state is above the ground level by 141 893 cm^{-1}, in excellent agreement with the MR-MP prediction of 141 916 cm^{-1}, a deviation of only 0.02%. However, the MR-MP theory predicts the fine-structure levels $^3P^o_1$ and $^3P^o_2$ to lie, respectively, 6 cm^{-1} and 4 cm^{-1} above the $^3P^o_0$, whereas they are assigned to lie, respectively, 122 cm^{-1} and 129 cm^{-1} below it. Large-scale MCDF calculations [33] also predict the $^3P^o_{1,2}$ fine-structure components to be above the $^3P^o_0$, agreeing with our MCDFB and MR-MP predictions. Thus the experimental assignment of the ordering and intervals of the fine-structure levels is suspect. Reexamination of the experimental data or further precision measurement is needed to resolve the discrepancy.

Figure 2 displays the theoretical-experimental deviations (cm^{-1}) in term energy separations of the lowest 29 excited levels (excluding the $3p^4\ ^1D_2$ and $3p^4\ ^1S_0$ states) plotted against the state numbers to magnify the remaining discrepancies. The figure clearly reveals that even the large-scale MCDF calculations of Kohstall *et al.*, including as many as 5 300 CSFs arising from the $n=3$–5 shells, fail to reproduce

TABLE II. Comparison of our MCDFB and MR-MP calculated energy separations, ΔE, and fine-structure separations, FS, with experimental data [34], and values from the MCDF calculations by Huang [7] and by Kohstall *et al.* [33] in siliconlike Ar^{4+}.

	State	MCDFB		Huang		Kohstall *et al.*		MR-MP		NIST	
		ΔE	FS	ΔE	FS	ΔE	FS	ΔE	FS	ΔE	FS
$3s^2 3p^2$											
1	$^3P_0$	0		0		0	0	0	0	0	0
2	$^3P_1$	741	741	810	810	750	750	757	757	765	765
3	$^3P_2$	2003	2003	2063	2063	2000	2000	2020	2020	2029	2029
4	$^1D_2$	18934		19113		16636		16275		16299	
5	$^1S_0$	41505		41842		38592		38054		37912	
$3s3p^3$											
6	$^5S_2^o$	81505		82100		84647		85819 (−2.04)		84100 [a]	
7	$^3D_1^o$	121292	0	121558	0	121313	0	121519 (0.09)	0	121630	0
8	$^3D_2^o$	121364	72	121711	153	121358	45	121568 (0.09)	49	121675	45
9	$^3D_3^o$	121528	236	121777	219	121540	227	121700 (0.08)	181	121803	173
10	$^3P_0^o$	142601	0	143041	0	141910	0	141916 (−0.02)	0	141893 [b]	0
11	$^3P_1^o$	142623	22	143284	243	141963	53	141922 (−0.11)	6	141771	−122
12	$^3P_2^o$	142650	49	143292	251	141983	73	141920 (−0.11)	4	141764 [b]	−129
13	$^1D_2^o$	156032 [c]		156052 [c]		154470 [c]		154275 [c] (−0.04)		154212	
17	$^3S_1^o$	198135		197402		198043		191111 (0.22)		191536	
18	$^1P_1^o$	204373		204177		194939		194641 (0.37)		195358	
$3s^2 3p3d$											
14	$^3F_2^o$	190610	0	191129	0	186856	0	186714	0		
15	$^3F_3^o$	191324	714	191976	847	187549	693	187422	708		
16	$^3F_4^o$	192313	1703	192480	1351	188375	1520	188403	1689		
19	$^3P_2^o$	224703	0	225345	0	219592	0	217797 (−0.10)	0	217572	0
20	$^3P_1^o$	225374	671	226303	958	220252	660	218489 (−0.09)	692	218284	712
21	$^3P_0^o$	225718	1015	225602	−701	220352	760	218835 (−0.09)	1038	218647	1075
22	$^1D_2^o$	231379 [d]		234202 [d]		226888 [d]		221273 [d] (0.24)		221815	
23	$^3D_1^o$	233069	0	233635	0	226542	0	224532 (−0.14)	0	224221	0
24	$^3D_2^o$	233329	260	232137	−1498	225020	−1522	224811 (−0.14)	279	224498	277
25	$^3D_3^o$	233522	453	234303	668	226985	441	225034 (−0.14)	502	224706	485
26	$^1F_3^o$	257452		257482		248074		245472 (−0.06)		245329	
27	$^1P_1^o$	264171		265457		256305		253871 (−0.69)		252141	
$3p^4$											
28	$^3P_2$	264668	0					264308 (0.05)	0	264427	0
29	$^3P_1$	265793	1125					265460 (0.05)	1152	265589	1162
30	$^3P_0$	266286	1618					265950 (0.05)	1642	266076	1649
31	$^1D_2$	274242						271405 (−18.77)		228519	
32	$^1S_0$	316697						311996 (3.96)		324864	

[a]Reference [36] gives 85 823 cm^{-1} for $^5S_2^o$.

[b]Reference [32] gives the values 141 773 cm^{-1} for $^3P_0^o$, and 141 764 cm^{-1} for $^3P_2^o$. The value for $^3P_1^o$ is not given.

[c]The dominant CSF in MCDFB approximation is $3s^2 3p3d$, but it is nominally represented as $3s3p^3$ for comparison.

[d]The dominant CSF in MCDFB approximation is $3s3p^3$, but it is nominally represented as $3s^2 3p3d$ for comparison.

the experimental term energy separations as accurately as does the MR-MP theory. Absolute deviations between MCDF and experiment increase progressively as term energy separation increases, primarily because MCDF, even on a large scale, cannot accurately account for dynamic correlation. The MR-MP theory can, however, and thus the deviations between the MR-MP theory and experiment remain nearly constant (of the order of 100 cm^{-1}) making accurate prediction of a large number of excited levels possible. The remaining deviations from the experiment of the MR-MP separations are most likely due to small variations in the quality of the state-averaged MCDFB SCF zero-order wave

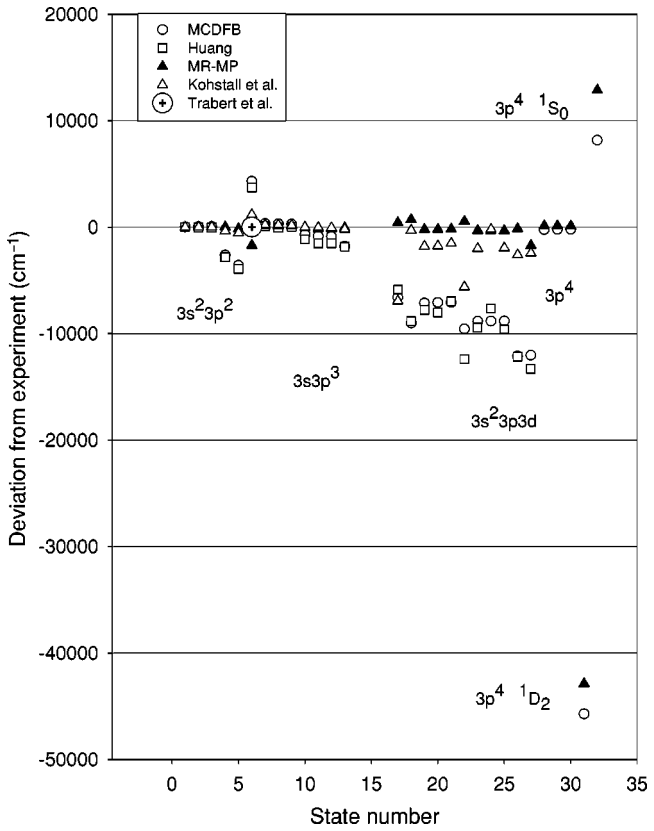

FIG. 1. Deviation from the experiment [34] (in cm^{-1}) of our MCDFB and MR-MP calculated energy separations and MCDF separations of Huang [7] and Kohstall *et al.* [33] for siliconlike Ar^{4+}. The circled plus sign represents the deviation between the beam-foil experiment of Träbert et al. [36] and our MR-MP theory.

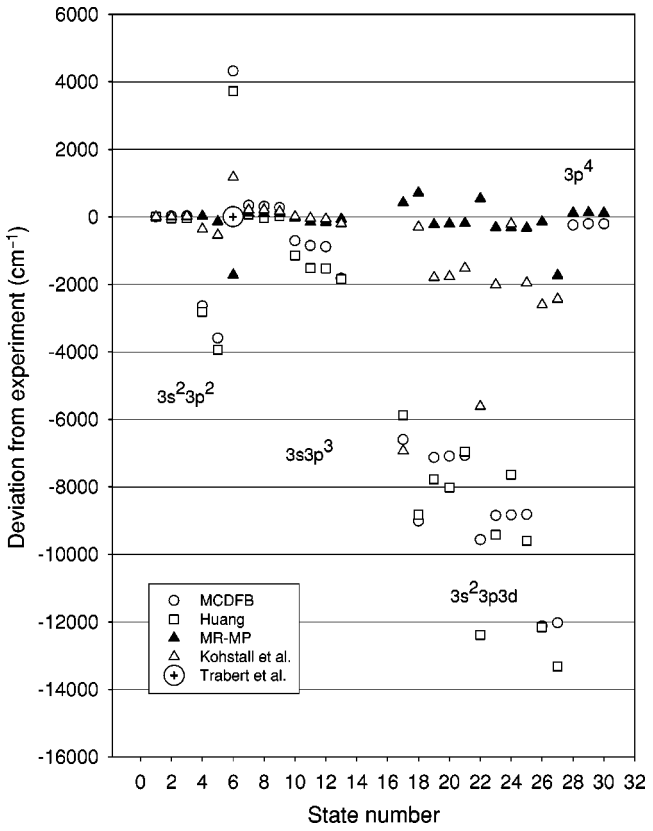

FIG. 2. Deviation from the experiment [34] (in cm^{-1}) of our MCDFB and MR-MP calculated energy separations and the MCDF separations of Huang [7] and Kohstall *et al.* [33] for siliconlike Ar^{4+}. The MCDFB and MR-MP values for the $3p^4\ ^1D_2$ and $^1S_0$ have been removed to obtain a more detailed picture. The circled plus sign represents the deviation between the beam-foil experiment of Träbert *et al.* [36] and our MR-MP theory.

functions. Noticeable discrepancies, ranging from 0.22% to 0.69% (Fig. 2), remain in $3s3p^3\ ^3S_1^o$ (state number 17), $3s3p^3\ ^1P_1^o$ (state number 18), $3s^23p3d\ ^1D_2^o$ (state number 22), $3s^23p3d\ ^1P_1^o$ (state number 27), in addition to $3s3p^3\ ^5S_2^o$ discussed earlier. The source of the discrepancies in the first four cases is not immediately apparent.

We have also predicted term energies of a large number of hitherto unobserved excited levels. Theoretical predictions of these may assist in assigning the spectra. The term energies and fine-structure intervals of the $3s^23p3d\ ^3F_{2,3,4}^o$ levels are given in Table III. An additional 65 excited levels arising from the nominal configurations $3s3p^23d$ and $3s^23d^2$ are displayed in Table III. We expect the predicted excitation energies to be accurate to well within 0.2%.

Figure 3 displays theory-experiment deviations (cm^{-1}) between fine-structure intervals in order to focus attention on the few anomalies. The deviations are plotted against the interval number in increasing order in the FS intervals as they appear from top to bottom in Table II. The bulk of the experimentally determined fine-structure intervals is reproduced by our MCDFB and by the large-scale MCDF calculations of Kohstall *et al.* MCDF accounts for the nondynamic correlation. The MR-MP theory, which recovers almost all dynamic correlations, further improves the agreement. Huang's MCDF values are seen to deviate noticeably from the experiment. The $3s^23p3d\ ^3P_0^o$-$^3P_2^o$ fine-structure separation (FS number 8 in Fig. 3), in particular, exhibits large deviation. Theoretical $3s^23p3d\ ^3D_2^o$-$^3D_1^o$ fine-structure intervals (FS number 9) computed by Huang and Kohstall *et al.* also deviate significantly the from the MR-MP theory and experiment, which are in good agreement. The figure also stresses the discrepancies discussed earlier between the experiment and MR-MP theory. The experimental fine-structure intervals $3s3p^3\ ^3P_1^o$-$^3P_0^o$ and $^3P_2^o$-$^3P_0^o$ (FS number 5 and 6) seriously contradict the theoretical intervals predicted by the MR-MP theory and by Kohstall's large-scale MCDF.

B. Term energies and fine-structure separations in aluminumlike iron

In Table IV, a detailed comparison of theoretical and experimental data is made on the term energy separations (ΔE) of the lowest 39 excited states relative to the ground $\mathcal{J}=1/2$ ($3s^23p\ ^2P_{1/2}^o$) odd-parity state. In the first column of the table, 40 theoretically determined states including the ground level are numbered in order of increasing energy. Theoretical MCDFB term energy separations and fine-structure intervals computed in this study and in that of Safronova *et al.* [6] are displayed in the third through sixth

TABLE III. Calculated MCDFB and MR-MP term energy separations of the energy levels arising from the configurations $3s3p^2 3d$ and $3s^2 3d^2$ in siliconlike Ar^{4+} (cm^{-1}).

State	MCDFB	MR-MP	State	MCDFB	MR-MP	State	MCDFB	MR-MP
$3s3p^2 3d$			$3s3p^2 3d$			$3s3p^2 3d$		
$^5F_1$	273813	274649	$^3G_5$	337476	327430	$^3F_2$	381957	371938
$^5F_2$	274064	274889	$^1G_4$	341110	334270	$^3F_3$	382177	372150
$^5F_3$	274450	275254	$^3D_1$	344561	334944	$^3F_4$	382513	372494
$^5F_4$	274979	275750	$^3D_2$	344690	335054	$^3D_3$	404340	384177
$^5F_5$	275664	276384	$^3D_3$	344850	335202	$^3D_2$	405054	384757
$^5D_0$	281198	283618	$^1F_3$	348597	339940	$^3D_1$	406060	395032
$^5D_1$	281270	283682	$^3F_2$	356904	348723	$^1S_0$	407178	389823
$^5D_2$	281414	283809	$^3F_3$	357449	349232	$^1D_2$	422033	403848
$^5D_3$	281631	284004	$^3F_4$	358215	349896	$^1P_1$	422788	411270
$^5D_4$	281926	284273	$^3D_1$	358399	351011	$^3P_2$	423674	410825
$^3F_2$	295392	294592	$^3D_2$	358628	351247	$^3P_1$	423742	412185
$^3F_3$	295860	295035	$^3D_3$	359003	351631	$^3P_0$	437301	419365
$^3F_4$	296506	295652	$^3P_0$	361995	355005	$^1F_3$	441341	422799
$^5P_3$	311529	307775	$^3P_1$	362995	355122	$^1D_2$	460979	437381
$^5P_2$	312036	308264	$^3S_1$	362543	355540	$3s^2 3d^2$		
$^5P_1$	312365	308580	$^3P_2$	362525	353576	$^3F_4$	441378	422790
$^3P_2$	322645	320051	$^1P_1$	369200	361534	$^3F_3$	441393	422773
$^3P_1$	323669	321095	$^3D_1$	378653	366232	$^3F_2$	455105	431956
$^3P_0$	324244	321665	$^3D_2$	379039	366719	$^1G_4$	455262	434583
$^3G_3$	337219	327373	$^3D_3$	380141	367440	$^3P_0$	460979	437381
$^3G_4$	337332	327472	$^1D_2$	380630	370064	$^3P_1$	461039	437435
						$^3P_2$	461152	437535
						$^1D_2$	464330	445362
						$^1S_0$	489183	468931

columns of the table. The seventh and eighth columns contain the term energy separations and fine-structure intervals computed in the MR-MP calculations. The term energy separations were computed by subtracting the total energy of the ground $3s^2 3p\ ^2P^o_{1/2}$ state from those of the excited levels. Experimental term energy separations and fine-structure intervals of the corresponding states compiled in the CHIANTI database [37] are reproduced in the last column for comparison. Values in parentheses next to the theoretical term energy separations are the percentage deviations between the experiment and MR-MP theory.

The MBPT term energy separations computed by Safronova *et al.* [6] agree well with our MR-MP theory and experiment for low-lying excited states. For the excited states arising from $3s^2 3d$ and $3s3p3d$ nominal configurations, however, the MBPT term energy separations deviate noticeably from the experiment. The MR-MP term energy separations in Table IV deviate from the experiment by 0.06% or less for all but two of the excited levels. Theoretical term energy separations agree closely enough with the experiment that deviations larger than a fraction of a percent are cause to question the experimental numbers. Deviations (in cm^{-1}) between the theory and experiment for the lowest 39 excited levels are plotted against the state number in Fig. 4. These showcase the accuracy of the MR-MP results and reveal a few notable discrepancies. Deviations between the experimental term energy separations and those computed in the *R*-matrix calculations by Storey *et al.* [38] (blank triangles) are seen to increase dramatically for higher excited states. Even excitations to the low-lying states arising from $3s3p^2$ and $3s^2 3d$ show large deviations due to inadequate recovery of dynamic correlation energy. Once dynamic correlation is accurately accounted for by state-specific MR-MP, term energies and fine-structure intervals are accurately reproduced. In Fig. 4, differences between the MR-MP term energy separations and experimental (filled triangles) are seen to be consistently small with two exceptions. For $3s3p[^3P]3d\ ^4P^o_{3/2}$ and $^4D^o_{7/2}$ (state numbers 25 and 28 in Table IV), the theory deviates from the experiment by 0.1%. The deviations are clear in the figure, one above and the other below the zero line, and experimental assignments of these terms are therefore suspect.

Table V displays seven $3s3p[^3P]3d$ excited states (state numbers 22 through 28 in Table IV) including the two levels just cited above. In the first column of the Table V, state numbers from Table IV are given. Theoretically determined term types and corresponding MR-MP term energy of each of the seven levels are given, respectively, in the second and third columns in order of increasing energy. In the last column, experimental term energies and accompanying term types are again displayed, this time in order of increasing energy, not in matching electronic terms as in Table IV. Computed and experimental term energies displayed in ascending order are now in excellent agreement, and the largest

percentage deviation between the theory and experiment is only 0.01%. However, experimental term types of the $^4D^o_{7/2}$ and $^4P^o_{3/2}$ are reversed from their theoretical designations. Figure 5 displays deviations (cm^{-1}) between the theory and experiment of the fine-structure intervals. These again point out the accuracy provided by the MR-MP theory and reveal a few discrepancies. Experimental and theoretical $3s3p[^3P]3d\,^4P^o_{3/2}$-$^4P^o_{5/2}$ and $3s3p[^3P]3d\,^4D^o_{7/2}$-$^4D^o_{3/2}$ fine-structure intervals disagree. We argue again that experimental term assignments of these two levels are incorrect. Another noticeable discrepancy revealed in the figure lies with the $3p^3\,^2P^o_{3/2}$-$^2P^o_{1/2}$ fine-structure interval (between the state numbers 17 and 18). We cannot assign the source of this discrepancy.

In addition to the excited levels compiled in the CHIANTI database, theoretical predictions have been made on the term energies of a large number of hitherto unobserved excited levels to aid experimental identification. An additional 44 excited levels arising from the nominal configurations, $3p^23d$ and $3s3d^2$, are displayed in Table VI. We expect that the predicted MR-MP excitation energies are accurate to well within 0.1%.

C. Magnetic dipole and electric quadrupole transition probabilities between the $3s^23p^{1\,2}P_{3/2,1/2}$ fine-structure states of aluminumlike iron and manganese

Magnetic dipole ($M1$) transitions of atomic ions are the origin of a number of low-density solar coronal and terrestrial plasma [31] lines. Thus studies of $M1$ transitions are of importance in the diagnostics of these lines. Recent relativistic MBPT studies by Johnson, Plante, and Sapirstein [4] on heliumlike ions have laid the foundation for high accuracy calculations of reduced matrix elements and transition rates in one- and two-valence-electron systems and demonstrated the capacity of theoretical methods to predict $E1$ and $M1$ transition rates accurately.

The $3s^23p^{1\,2}P^o_{3/2}$-$^2P^o_{1/2}$ decay rates of aluminumlike manganese and iron were determined first by Moehs and Church in a Kingdon ion trap experiment [14,15]. In the present study, we have employed our relativistic MCDFB plus MR-MP method to calculate the energy levels of the $3s^23p^{1\,2}P_{\mathcal{J}}$ ($\mathcal{J}=1/2,3/2$) fine-structure states. Transition probabilities between the two levels, and the lifetime of the $^2P^o_{3/2}$ fine-structure level, were evaluated following the method outlined in Sec. II. Table VII displays the $M1$ and $E2$ transition probabilities, computed in the Babushkin gauge, and lifetimes computed with state-averaged MCDFB and state-specific MR-MP wave functions. Because of strong coupling between the large and small components of the Dirac four-spinors in the transition matrix elements, $E2$ transition probabilities evaluated by excluding the negative-energy space in the Coulomb gauge are inaccurate and thus deviate from the values evaluated in the Babushkin gauge [39]. When contributions from the negative-energy space are included, transition probabilities evaluated in the Coulomb gauge approach those evaluated in the Babushkin gauge. $M1$ and $E2$ transition probabilities computed with MR-MP wave functions excluding [DCB(+)] and including [DCB(+,−)] negative-energy states appear, respectively, in the fourth and fifth columns. The transition probabilities evaluated with and without negative-energy states in the Babushkin gauge differ very little, indicating that transition probabilities in this gauge are less sensitive to the negative-energy contribution. The fine-structure intervals (Table IV) and transition probabilities computed with MCDFB and MR-MP wave functions agree well, indicating that dynamical correlation differences are minor in transition probabilities of highly ionized ions. The $M1$ transition probabilities are three orders of magnitude larger than the $E2$, indicating that radiative decay of the $^2P_{3/2}$ state occurs predominantly via M1 transition.

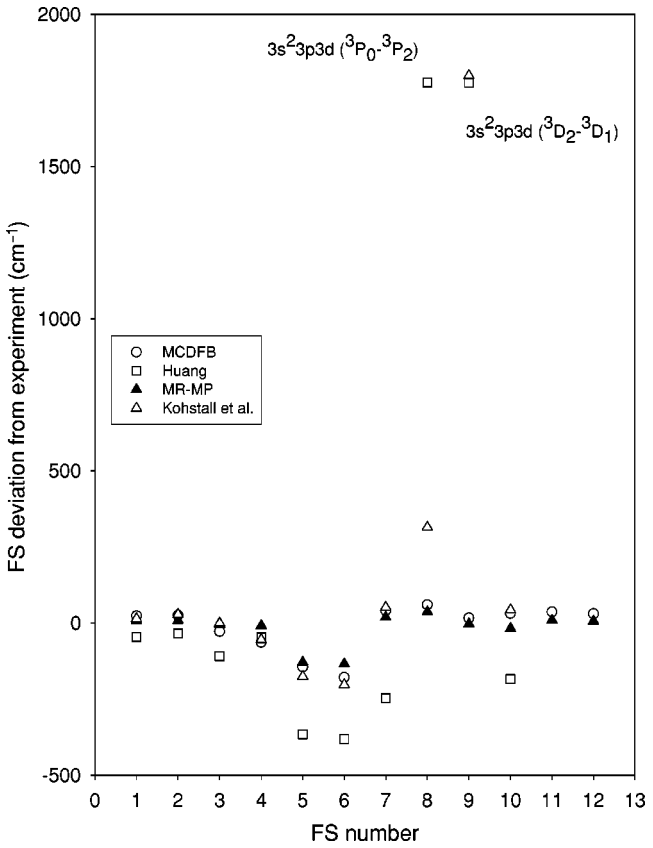

FIG. 3. Deviation (in cm^{-1}) from the experiment [34] of our MCDFB and MR-MP calculated fine-structure separations, plus the MCDF values calculated by Huang [7] and by Kohstall *et al.* [33] in siliconlike Ar^{4+}.

Table VIII compares theoretical lifetimes with the experiment. The MR-MP theoretical lifetime, 31.11 ms, of the $^2P^o_{3/2}$ level of Mn^{12+} agrees well with the theoretical lifetime computed by Huang [7], and with the experimental value, 31.32 ± 1.82 ms, obtained by Moehs and Church [14,15]. The theory and the Kingdon trap experiment [14,15] also agree well on the lifetime of the $2s^22p^{4\,3}P_1$ state of oxygenlike argon. Here the theoretical lifetime, 14.99 ms [40], is in very good agreement with the experiment (14.8 ± 0.48 ms).

The MR-MP theoretical lifetime, 16.61 ms, of the $^2P^o_{3/2}$ state of Fe^{13+} agrees well with the theoretical lifetimes computed by Huang [7] and Storey *et al.* [38], but not with the MCHF [41] calculated lifetime. The MR-MP lifetime also agrees, to within the experimental error, with the recent ex-

TABLE IV. Comparison of our MCDFB and second-order MR-MP calculated energy separations, ΔE, and fine-structure separations, FS, with experimental data [37], and with values from the MBPT calculations by Safronova *et al.* [6] in aluminumlike Fe^{13+}. All energies are in cm^{-1}.

	State	MCDFB		Safronova *et al.*		MR-MP		CHIANTI	
		ΔE	FS	ΔE	FS	ΔE	FS	ΔE	FS
$3s^2 3p$									
1	$^2P^o_{1/2}$	0	0	0	0	0	0	0	0
2	$^2P^o_{3/2}$	18781	18781	18831	18831	18859	18859	18852	18852
$3s3p^2$									
3	$^4P_{1/2}$	222633	0	225187	0	225094 (0.01)	0	225113	0
4	$^4P_{3/2}$	230246	7613	232889	7702	232801 (0.01)	7707	232788	7675
5	$^4P_{5/2}$	239889	17256	242451	17264	242396 (−0.00)	17302	242387	17274
6	$^2D_{3/2}$	300283	0	298903	0	299192 (0.02)	0	299241	0
7	$^2D_{5/2}$	302467	2184	301126	2223	301416 (0.02)	2224	301468	2227
8	$^2S_{1/2}$	370478		364267		364643 (0.01)		364692	
9	$^2P_{1/2}$	395156	0	388057	0	388289 (0.06)	0	388508	0
10	$^2P_{3/2}$	403425	8269	396052	7995	396268 (0.06)	7979	396511	8003
$3s^2 3d$									
11	$^2D_{3/2}$	482690	0	472279	0	473290 (−0.01)	0	473222	0
12	$^2D_{5/2}$	484514	1824	474242	1963	475268 (−0.01)	1978	475201	1979
$3p^3$									
13	$^2D^o_{3/2}$	576283	0	576068	0	576475 (−0.02)	0	576382	0
14	$^2D^o_{5/2}$	579827	3544	579912	3844	580295 (−0.01)	3820	580231	3849
15	$^4S^o_{3/2}$	591044		588844		588991 (0.00)		589000	
17	$^2P^o_{1/2}$	646930	0	641696	0	642277 (−0.02)	0	642178	0
18	$^2P^o_{3/2}$	650107	3177	645244	3548	645776 (−0.06)	3499	645420	3242
$3s3p[^3P]3d$									
16	$^4F^o_{3/2}$	642059		641239		641837			
19	$^4F^o_{5/2}$	646108	0	645313	0	645905 (0.01)	0	645987	0
20	$^4F^o_{7/2}$	652025	5917	651223	5910	651837 (0.02)	5932	651944	5957
21	$^4F^o_{9/2}$	660288	14180	659539	14226	660165 (0.01)	14260	660261	14274
22	$^4P^o_{5/2}$	692870	0	689678	0	690289 (0.00)	0	690301	0
25	$^4P^o_{3/2}$	706653	13783	692051	2372	703349 (0.12)	13060	704208 [a]	13907
26	$^4P^o_{1/2}$	706033	13163	693557	3879	703737 (0.00)	13448	703748	13447
23	$^4D^o_{3/2}$	695565	0	703580	0	692665 (−0.00)	0	692660	0
24	$^4D^o_{1/2}$	697441	1876	703197	−383	694162 (0.00)	1497	694167	1507
27	$^4D^o_{5/2}$	707142	11577	703500	−80	704099 (0.00)	11434	704112	11452
28	$^4D^o_{7/2}$	706798	11233	702727	−853	704134 (−0.11)	11469	703391 [a]	10731
29	$^2D^o_{3/2}$	722748	0	716538	0	717234 (−0.01)	0	717193	0
30	$^2D^o_{5/2}$	723271	523	717163	625	717852 (0.00)	618	717859	666
31	$^2F^o_{5/2}$	754156	0	743733	0	744914 (0.01)	0	744963	0
32	$^2F^o_{7/2}$	769061	14905	758566	14833	759796 (0.00)	14882	759812	14849
33	$^2P^o_{3/2}$	820610	0	806112	0	807316 (−0.02)	0	807111	0
34	$^2P^o_{1/2}$	828684	8074	814018	7969	815352 (−0.03)	8036	815123	8012
$3s3p[^1P]3d$									
35	$^2F^o_{7/2}$	833369	0	815939	0	817722 (−0.02)	0	817591	0
36	$^2F^o_{5/2}$	836461	3092	818947	3008	820730 (−0.02)	3008	820599	3008
37	$^2P^o_{1/2}$	856261	0	837739	0	839453 (0.00)	0	839490	0
39	$^2P^o_{3/2}$	860112	3851	839172	1433	843646 (0.00)	4193	843653	4163
38	$^2D^o_{3/2}$	857065	0	842226	0	840993 (−0.03)	0	840773	0
40	$^2D^o_{5/2}$	860297	3232	843273	1047	844686 (−0.02)	3693	844475	3702

[a]Experimental assigments of $^4P^o_{3/2}$ and $^4D^o_{7/2}$ have been interchanged (see Table V for details).

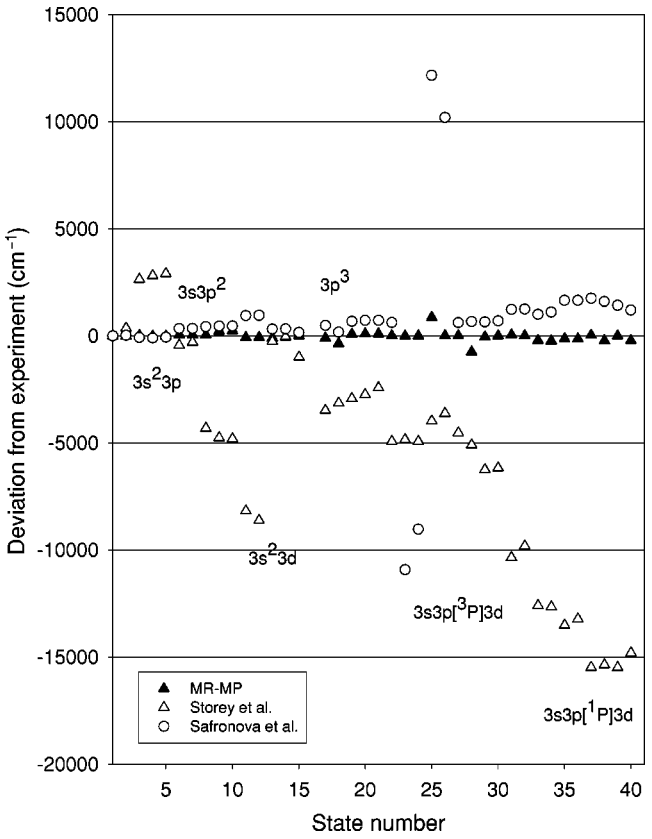

FIG. 4. Deviation (in cm^{-1}) from the experiment [37] of our MR-MP calculated energy separations, and the calculated values of Storey *et al.* [38] and Safronova *et al.* [6] for aluminumlike Fe^{13+}.

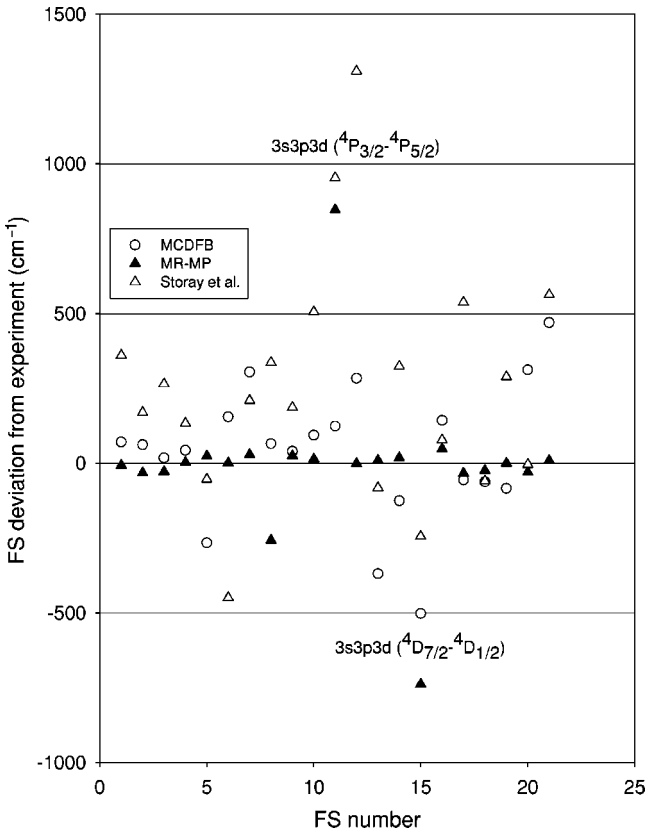

FIG. 5. Deviation (in cm^{-1}) from the experiment [37] of our MCDFB and MR-MP calculated fine-structure separations, and the calculated values of Storey *et al.* [38] for aluminumlike Fe^{13+}.

perimental value (16.74 ± 0.12 ms) obtained by Beiersdorfer *et al.* using the Livermore EBIT [13], but deviates noticeably from the value (17.52 ± 0.29 ms) obtained by Church and co-worker [14,15] in their Kingdon trap experiment. The MR-MP theory tends to agree more with the recent EBIT lifetime measurements for other ions as well. Theoretical $M1$ lifetimes for the $^3P_2^o$ state of berylliumlike, the $^2P_{3/2}^o$ state of boronlike, and the $^2P_{1/2}^o$ state of fluorinelike Ar ions [40], respectively, 15.66 ms, 9.59 ms, and 9.45 ms, agree to within the experimental error with a recent Livermore EBIT experiment which yielded, respectively, 15.0 ± 0.8 ms, 9.70 ± 0.15 ms and 9.32 ± 0.12 ms [42].

TABLE V. Proposed reassignment of $3s3p[^3P]3d\,^4P$ and ^4D J states of aluminumlike Fe^{13+}. The energy levels are arranged in ascending order of our second-order MR-MP results. The experimental data were taken from the CHIANTI atomic database [37]. The assignment of experimental energy levels is indicated to the right of the experimental data. All values are in cm^{-1}.

Number	State	MR-MP	CHIANTI	State
22	$^4P_{5/2}^o$	690289	690301	$^4P_{5/2}^o$
23	$^4D_{3/2}^o$	692665	692660	$^4D_{3/2}^o$
24	$^4D_{1/2}^o$	694162	694167	$^4D_{1/2}^o$
25	$^4P_{3/2}^o$	703349	703391	$^4D_{7/2}^o$
26	$^4P_{1/2}^o$	703737	703748	$^4P_{1/2}^o$
27	$^4D_{5/2}^o$	704099	704112	$^4D_{5/2}^o$
28	$^4D_{7/2}^o$	704134	704208	$^4P_{3/2}^o$

IV. CONCLUSION

We have developed and implemented a straightforward relativistic MR-MP method capable of accurately predicting transition energies and transition rates for systems with multiple valence electrons. These are difficult both experimentally and theoretically because they typically display a number of nearly degenerate low-lying excited states. Applications to berylliumlike through sulfurlike argon ions, and aluminumlike and siliconlike iron and manganese, have established the accuracy of the method [40]. In this study, theoretical calculations on siliconlike argon and aluminumlike iron have been reported, and they demonstrate unprecedented accuracy. Term energy separations and fine structure intervals in complex ions with multiple valence-shell electrons ($\geqslant 2$) have been obtained to within a fraction of a percent for a large number of excited levels by the theory. The calculated MR-MP transition energies for Ar^{4+} and Fe^{13+} are the most accurate among those obtained by a variety of relativistic methods. The crucial components are a fully relativistic many-body theory that accounts for one-

TABLE VI. MCDFB and MR-MP energy levels of the even-parity $3p^2 3d$ and $3s3d^2$ configurations of aluminumlike Fe^{13+}. All energies are in cm^{-1}.

State	MCDFB	MR-MP
$3p^2 3d$		
$^2F_{5/2}$	963200	960889
$^2F_{7/2}$	969900	967691
$^4F_{3/2}$	972241	966037
$^4F_{5/2}$	976755	970693
$^4F_{7/2}$	982880	976961
$^2P_{3/2}$	988179	983988
$^4F_{9/2}$	989784	983604
$^2P_{1/2}$	992852	988301
$^4D_{3/2}$	1000230	995427
$^4D_{5/2}$	1001061	996003
$^4D_{1/2}$	1007475	1003465
$^4D_{7/2}$	1007674	1002947
$^2G_{7/2}$	1026585	1015917
$^2G_{9/2}$	1030462	1020067
$^2D_{5/2}$	1045779	1033523
$^2D_{3/2}$	1049356	1037695
$^4P_{5/2}$	1057335	1044698
$^4P_{1/2}$	1058116	1044829
$^4P_{3/2}$	1058174	1044127
$^2P_{1/2}$	1089341	1076679
$^2P_{3/2}$	1092544	1078329
$^2S_{1/2}$	1100442	1089810
$^2D_{3/2}$	1104956	1087195
$^2D_{5/2}$	1115749	1095714
$^2F_{5/2}$	1119083	1099992
$^2F_{7/2}$	1124270	1105117
$^2D_{5/2}$	1186709	1150013
$^2D_{3/2}$	1192141	1155852
$3s3d^2$		
$^4F_{3/2}$	1131928	1124030
$^4F_{5/2}$	1132722	1124835
$^4F_{7/2}$	1133812	1125945
$^4F_{9/2}$	1135178	1127373
$^4P_{1/2}$	1167310	1158354
$^4P_{3/2}$	1167793	1158863
$^4P_{5/2}$	1168430	1159538
$^2D_{5/2}$	1221903	1197986
$^2D_{3/2}$	1222633	1197372
$^2G_{7/2}$	1222927	1199202
$^2G_{9/2}$	1223270	1199423
$^2F_{5/2}$	1274240	1242616
$^2F_{7/2}$	1275182	1243842
$^2S_{1/2}$	1300238	1275073
$^2P_{1/2}$	1317708	1274120
$^2P_{3/2}$	1319618	1275727

body kinematic relativistic effects, relativistic nondynamic and dynamic correlation corrections, and Lamb shift corrections. The correlation corrections due to contributions of the Coulomb and Breit interactions to the $M1$ and $E2$ transition operators have been accounted for in the first-order MR-MP wave functions. Where deviation between the theory and experiment is significant, of the order of a percent or larger, the theory is able to challenge the validity of the spectroscopic assignments. The current level of relativistic many-body theory is capable of predicting lifetimes of excited levels comparable in accuracy to the experimental lifetime measurements.

TABLE VII. $M1$ and $E2$ transition probabilities (in s^{-1}) and lifetimes (in milliseconds) of $3s^2 3p\ ^2P^o_{3/2}$ state in aluminumlike Mn^{12+} and Fe^{13+} ions.

Transition		MCDFB	MR-MP	
			DCB(+)	DCB(+,−)
Mn^{12+}				
$^2P^o_{1/2}$-$^2P^o_{3/2}$	$M1$	32.14	32.14	32.14
$^2P^o_{1/2}$-$^2P^o_{3/2}$	$E2$	0.0065	0.0065	0.065
$\tau\ ^2P^o_{3/2}$		31.11	31.11	31.11
Fe^{13+}				
$^2P^o_{1/2}$-$^2P^o_{3/2}$	$M1$	60.18	60.18	60.17
$^2P^o_{1/2}$-$^2P^o_{3/2}$	$E2$	0.01457	0.01463	0.01463
$\tau\ ^2P^o_{3/2}$		16.61	16.61	16.61

Because core and valence-shell spinors are optimized for the average energy over a number of low-lying states with different $\mathcal{J}$ and parity, the state-averaged MCDFB energy for a given state is slightly higher than the state-specific MCDFB energy. However, the subsequent state-specific MR-MP perturbation calculations based on the single set of MCDFB core, valence, and virtual spinors accurately reproduce the differences in dynamic correlation corrections among individual states, resulting in accurate term energy and fine-structure separations for all states included in the state-averaged MCDF. The key to successful implementation lies in the optimization of a single set of spinors within the state-averaged MCDFB energy to account for nondynamic correlation (quasidegeneracy), and then subsequent state-

TABLE VIII. Comparison of the theoretical and experimental lifetimes (milliseconds) of the $3s^2 3p\ ^2P^o_{3/2}$ state in Mn^{12+} and Fe^{13+} ions.

	Mn^{12+}	Fe^{13+}
Storey *et al.* [38]		16.60
Huang [7]	31.07	16.66
MCHF [41]		19.6
MR-MP	31.11	16.61
Experiment		
References [14,15]	31.32±1.82	17.52±0.29
Reference [13]		16.74±0.12

[a]Rescaled value using experimental wavelength is 16.60 ms.

specific MR-MP perturbation calculations to accurately account for dynamic correlation for individual states. This is the crucial departure from our earlier relativistic MR-MP theory, where state-specific MCDFB SCF was employed [20]. The successful implementation emphasizes that once nondynamic correlation is accounted for by MCDF or CI, the bulk of the remaining electron correlation is pair correlation, which may be accurately accounted for by multireference second-order perturbation theory.

ACKNOWLEDGMENT

This research is supported in part by the U.S.-Israel Binational Science Foundation.

[1] D.J. Bieber, H.S. Margolis, P.K. Oxley, and J.D. Silver, Phys. Scr., T **73**, 64 (1997).
[2] E. Träbert, Can. J. Phys. **80**, 1481 (2002).
[3] E. Lindroth and S. Salomonson, Phys. Rev. A **41**, 4659 (1990).
[4] W.R. Johnson, D.R. Plante, and J. Sapirstein, Adv. At., Mol., Opt. Phys. **35**, 255 (1995).
[5] U.I. Safronova, C. Namba, I. Murakami, W.R. Johnson, and M.S. Safronova, Phys. Rev. A **64**, 012507 (2001).
[6] U.I. Safronova, C. Namba, J.R. Albritton, W.R. Johnson, and M.S. Safronova, Phys. Rev. A **65**, 022507 (2002).
[7] K.-N. Huang, At. Data Nucl. Data Tables **32**, 504 (1985).
[8] K.-N. Huang, At. Data Nucl. Data Tables **34**, 1 (1986).
[9] E.B. Saloman and Y.-K. Kim, Phys. Rev. A **38**, 577 (1988).
[10] V.A. Dzuba, V.V. Flambaum, and M.G. Kozlov, Phys. Rev. A **54**, 3948 (1996).
[11] I.M. Savukov and W.R. Johnson, Phys. Rev. A **65**, 042503 (2002).
[12] Y. Ishikawa and M.J. Vilkas, Phys. Rev. A **63**, 042506 (2001).
[13] P. Beiersdorfer, E. Träbert, and E.H. Pinnington, Astrophys. J. **587**, 836 (2003).
[14] D.P. Moehs and D.A. Church, Phys. Rev. A **59**, 1884 (1999).
[15] D.P. Moehs and D.A. Church, Astrophys. J. **516**, L111 (1999).
[16] J. Sucher, Phys. Rev. A **22**, 348 (1980).
[17] M.H. Mittleman, Phys. Rev. A **24**, 1167 (1981).
[18] Y. Ishikawa and H.M. Quiney, Int. J. Quantum Chem., Symp. **21**, 523 (1987).
[19] M.J. Vilkas, Y. Ishikawa, and K. Koc, Phys. Rev. E **58**, 5096 (1998).
[20] M.J. Vilkas, Y. Ishikawa, and K. Koc, Phys. Rev. A **60**, 2808 (1999).
[21] K. Hirao, Chem. Phys. Lett. **190**, 374 (1992).
[22] K. Hirao, Chem. Phys. Lett. **201**, 59 (1993).
[23] E. Eliav, U. Kaldor, and Y. Ishikawa, Phys. Rev. A **49**, 1724 (1994).
[24] C. Møller and M.S. Plesset, Phys. Rev. **46**, 618 (1934).
[25] M.J. Vilkas, K. Koc, and Y. Ishikawa, Chem. Phys. Lett. **296**, 68 (1998).
[26] Y. Ishikawa and K. Koc, Phys. Rev. A **50**, 4733 (1994).
[27] P. Indelicato, O. Gorceix, and J.P. Desclaux, J. Phys. B **20**, 651 (1987).
[28] Y.-K. Kim, in *Atomic Processes in Plasmas*, edited by Yong Ki-Kim and Raymond C. Elton, AIP Conf. Proc. 206 (AIP, New York, 1990), p. 19.
[29] P.J. Mohr and Y.-K. Kim, Phys. Rev. A **45**, 2727 (1992).
[30] I.P. Grant, J. Phys. B **7**, 1458 (1974).
[31] E. Träbert, Phys. Scr., T **100**, 88 (2002).
[32] S. Bashkin and J.O. Stoner, *Atomic Energy Levels and Grotrian Diagrams* (North-Holland, Amsterdam/American Elsevier, New York, 1978), Vol. II, p. 241.
[33] C. Kohstall, S. Fritzsche, B. Fricke, and W.-D. Sepp, At. Data Nucl. Data Tables **70**, 63 (1998).
[34] J. R. Fuhr, D. E. Kelleher, W. C. Martin, A. Musgrove, J. Sugar, W. L. Wiese, G. R. Dalton, R. A. Dragoset, P. J. Mohr, K. Olsen, J. Reader, E. B. Saloman, C. J. Sansonetti, and G. Wiersma, *NIST Atomic Spectra Database* Ver. 2.0, March 1999, NIST Physical Reference Data. Available on-line at http://physics.nist.gov/PhysRefDat/contents.html
[35] E. Träbert, R. Hutton, L. Engström, S.L. Bliman, H.G. Berry, and C. Kurtz, Phys. Lett. A **129**, 381 (1988).
[36] E. Träbert, P.H. Heckmann, R. Hutton, and I. Martinson, J. Opt. Soc. Am. B **5**, 2173 (1988).
[37] K.P. Dere, E. Landi, H.E. Mason, B.C. Monsignori Fossi, and P.R. Young, Astron. Astrophys., Suppl. Ser. **125**, 149 (1997). Available on-line at http://wwwsolar.nrl.navy.mil/chianti.html
[38] P.J. Storey, H.E. Mason, and P.R. Young, Astron. Astrophys., Suppl. Ser. **141**, 28 (2000).
[39] J. Sapirstein (private communication).
[40] M.J. Vilkas and Y. Ishikawa (unpublished).
[41] Ch. Froese-Fischer and B. Liu, At. Data Nucl. Data Tables **34**, 261 (1986).
[42] E. Träbert, S.B. Utter, P. Beiersdorfer, G.V. Brown, H. Chen, C. Harris, P. Neill, D.W. Savin, and A.J. Smith, Astrophys. J. **541**, 506 (2000).